Int. J. Therm. Sci. (2001) 40, 638–648

S1290-0729(01)01253-4/FLA

Unsteady planar stagnation flow on a heated plate

Emilia-Cerna Mladin [a*], Jacques Padet [b]

[a] *Polytechnic University of Bucharest, Chair of Engineering Thermodynamics, Splaiul Independentei 313, 77206 Bucharest, Romania*

[b] *Universite de Reims Champagne-Ardenne, Faculte de Sciences, Moulin de Housse, B.P. 1039 – 51687 Reims cedex, France*

(Received 15 March 2000, accepted 15 September 2000)

Abstract — The present study presents a mathematical model that has been derived to reveal the influence of the thermal dynamics of the impinging plate on the hydrodynamic and thermal boundary layer thicknesses and Nusselt number for a planar stagnation flow, when incident velocity and/or applied heat flux are transient. The model consists of a system of three ordinary differential equations and an analytical solution for the temperature distribution across the plate. Results showed that the boundary layer thicknesses and Nusselt number were affected by the periodical variations in the applied heat flux to within 1%. By contrast, the temperature across the impinging plate had significant fluctuations induced by both forcing functions. The influence of various parameters on the plate temperature distribution was systematically assessed. Comparison of theoretical predictions with experimental measurements indicated an agreement to within 1% in temperature, heat flux, and Nusselt number at the impinging surface. © 2001 Éditions scientifiques et médicales Elsevier SAS

stagnation planar flow / unsteady heat transfer / transient convection / thermal coupling / nonlinear dynamics

Nomenclature

A	dimensionless coefficient $= a_p/(Cl_p^2)$	
B	dimensionless coefficient (equation (27))	
C	steady-state free stream velocity gradient	s^{-1}
C_t	instantaneous free stream velocity gradient	s^{-1}
C_*	dimensionless constant $= C_t w/V_i$	
f	forcing frequency of incident flow pulses	s^{-1}
f_q	forcing frequency of heat flux variations .	s^{-1}
f_*	dimensionless frequency $= f/C$	
f_{q*}	dimensionless frequency $= f_q/C$	
h	heat transfer coefficient	$W{\cdot}m^{-2}{\cdot}K^{-1}$
k	thermal conductivity	$W{\cdot}m^{-1}{\cdot}K^{-1}$
l_p	impinging plate thickness	m
Nu_w	instantaneous Nusselt number $= h \cdot w/k$	
Nu_*	$= Nu_w/Nu_0$	
q	heat flux applied to the plate (*figure 1*) . .	$W{\cdot}m^{-2}$
q_*	dimensionless heat flux (equation (19))	
q_s	heat flux leaving the plate (*figure 1*) . . .	$W{\cdot}m^{-2}$
q_{s*}	dimensionless surface heat flux (equation (5))	
Pr	Prandtl number evaluated at T_{f0}	
t	time	s
T	temperature	K
U_∞	local x-velocity in the freestream	$m{\cdot}s^{-1}$
$U_{\infty*}$	$= U_\infty/V_{i0}$	
V_∞	local y-velocity in the freestream	$m{\cdot}s^{-1}$
V_i	incident flow velocity	$m{\cdot}s^{-1}$
w	jet width or cylinder diameter	m
x	distance along the plate (*figure 1*)	m
x_*	dimensionless distance $= x/w$	
y	distance perpendicular to the plate (*figure 1*)	m
y_*	$= y/l_p$	
α_k	$= k_f^{-1}(T_{s0} - T_\infty)(\partial k_f/\partial T)\|_{T_{f0}}$	
a_p	plate diffusivity $= (k/\rho c_p)_{\text{plate}}$	$m^2{\cdot}s^{-1}$
α_ν	$= \nu_f^{-1}(T_{s0} - T_\infty)(\partial \nu_f/\partial T)\|_{T_{f0}}$	
β	dimensionless distance $= (y - l_p)/\Delta$	
Γ	dimensionless thickness $= C\Delta^2/\nu_{f0}$	
ε_1	dimensionless flow amplitude (equation (28))	
ε_2	dimensionless heat flux amplitude (equation (29))	
θ	$= (T - T_\infty)/(T_{s0} - T_\infty)$	
Λ	dimensionless thickness $= C\delta^2/\nu_{f0}$	
δ	instantaneous hydrodynamic boundary layer thickness	m

* Correspondence and reprints.

E-mail addresses: cerna@eeee.unesco.pub.ro (E.-C. Mladin), Jacques.Padet@univ-reims.fr (J. Padet).

Δ	instantaneous thermal boundary layer thickness	m
ν	kinematic viscosity	$m^2 \cdot s^{-1}$
τ	dimensionless time $= Ct$	

Subscripts

f	pertaining to film temperature $(T_s + T_\infty)/2$
0	pertaining to $t = 0$ and/or steady-state
p	pertaining to plate
s	pertaining to surface
∞	pertaining to freestream

1. INTRODUCTION

A related theoretical study demonstrated the opportunity to modify heat transfer rates due to the nonlinearities present in the equations governing the dynamical responses of the hydrodynamic and thermal boundary layers of a pulsating incident stagnation flow [1]. Several past experimental studies considered also a time dependent convective heat transfer in stagnation flows where the transients are induced by a periodic or impulsive motion in the free stream velocity. Results were reported when the time averaged Nusselt numbers were thus altered compared to the steady state cases.

Kasza [2] developed a mathematical model to study the thermal response of a two-dimensional, unsteady, laminar, incompressible, constant property boundary layer in the vicinity of a stagnation point. The temperatures of the fluid free stream and surface were assumed to be uniform and not dependent on time. Upon employing power series solutions to the conservation equations for momentum and energy, a system of two ordinary differential equations was obtained for the transient responses of the surface heat flux and wall shear stress. Sinusoidal pulsations in the incident free stream velocity yielded elevated surface heat fluxes. However, the imposed constant surface temperature in conjunction with a varying surface heat flux is physically restrictive and may account for the calculated enhancements.

Sheriff and Zumbrunnen [3] used intermittent ($\varepsilon_1 = 1$) water jets with Strouhal numbers greater than 0.26 to enhance heat transfer in the stagnation region by a periodic boundary layer renewal. Mladin and Zumbrunnen [4] produced pulsating air jets impinging onto a heated surface. Low Strouhal number (< 0.03) pulses lead at the stagnation line to a diminished heat transfer atributed to nonlinear dynamics effects. On the contrary, large Strouhal number (> 0.1)—large amplitude pulses indicated in the stagnation region elevated time averaged Nusselt numbers associated with surface renewal effects created by the impingement of some large coherent fluid structures onto the surface. In all such situations the nozzle to plate distances were kept small to avoid turbulence development. Thus, an opportunity to affect heat transfer rates in stagnation flows by inducing pulsations has been recently established. These cases are generally characterized by higher Strouhal numbers (St_w) and higher pulse magnitudes (ε_1). It should be noted that the influence of the impinging surface was not commented or even considered in none of these studies.

The present work continues the mathematical modeling developed by Mladin and Zumbrunnen [1] by including the transient conduction through the impinging plate. The previous model consisted of three ordinary differential equations that could provide the time-histories of the thermal and hydrodynamic boundary layer thicknesses and of impinging surface temperature. The heat flux leaving the surface was assumed in that model as a known forcing function. However, this heat flux is difficult to be known, especially for transient flows of small characteristic length, where a sensor may disturb the heat transfer condition. On the other side, microsensors capable of measuring instantaneous data are costly and need sometimes to be manufactured directly on the surface by use of special techniques [4]. Therefore, the present analysis considered situations when the known heat flux is applied at the bottom of the impinging plate. The heat flux leaving the surface results from the interaction between the plate thermophysical properties and geometry and the incident flow characteristics. Thus, the new model may provide realistic predictions for the heat flux at the impinging surface under different external conditions. The new approach improved the overall agreement of theoretical predictions with experimental measurements for surface temperature from 5% to 1%.

The stagnation region, which is considered in this study, is depicted in *figure 1*. Such flows arise beneath impinging planar or 'slot' jets, on a cylinder in a cross flow, or in the front stagnation region of any bluff body where the frontal surface can be effectively represented by a tangent plane. Although the incident flow velocities U_∞ and V_∞ may be unsteady, it is assumed that symmetry in the flow is preserved about the stagnation line ($x = 0$). The hydrodynamic and thermal boundary layers are thereby spatially constant in the vicinity of $x = 0$. The heat transfer condition at the bottom of the plate ($y = 0$) is specified by functions $q(t)$, while a heat flux $q_s(t)$ results at the impingement surface ($y = l_p$). Selected forcing functions for the incident pulsating flow velocity and periodic heat flux have been used so that they converge smoothly to the steady-state values as temporal variations

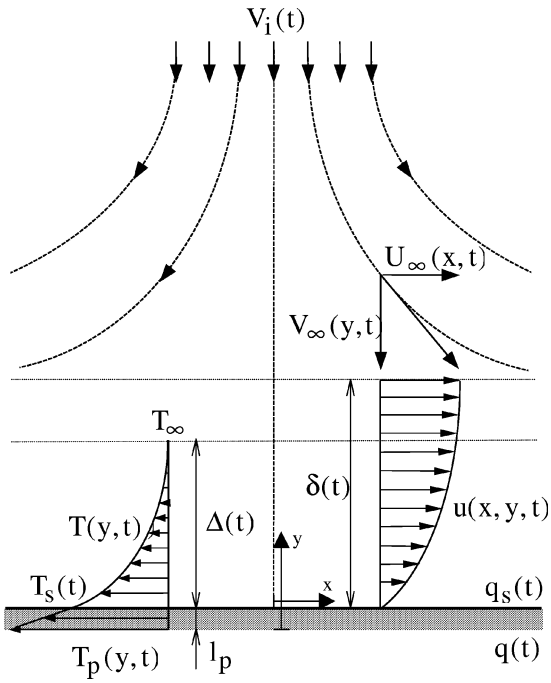

Figure 1. Unsteady planar stagnation flow on a heated plate.

become small. The temperature in the freestream, T_∞, is assumed to remain constant. It should be noted that theoretical and experimental studies have shown that the local heat transfer coefficient is spatially constant to within 1% over a distance equal to about one-half jet width from the stagnation line of a laminar planar jet with a uniform fluid discharge velocity across the nozzle width. This uniformity is attributable to the symmetry of the impinging flow and extends the validity of the theoretical analysis to regions away from the stagnation line.

2. ANALYSIS

Description of analytical method and assumptions

Consideration of transient effects in convection often precludes an exact analytical approach since transient terms that are routinely omitted in many convection studies must be retained. Where transient effects can be incorporated with similarity methods for example, restrictions are often necessary regarding functional relationships between variables [5]. The approach which was selected is related to the von Karman–Pohlhausen technique. Equations for momentum and energy conservation in their integral and differential forms were used with *temporally adaptive profiles* (expressed as polynomials with time dependent coefficients) for fluid velocity and temperature to obtain governing equations for the hydrodynamic and thermal boundary layer responses.

The problem was solved under a few general assumptions. For the flow, they are:

(i) incompressible laminar flow,
(ii) constant mass density and specific heat but possible temperature-dependent dynamic viscosity and thermal conductivity,
(iii) negligible viscous heating,
(iv) negligible body forces in comparison to viscous forces, and
(v) $\Delta \leqslant \delta$.

The last assumption restricts the model to fluids with Prandtl numbers greater than about unity. However, in a related study [6], results have been shown to remain accurate to within 2% for $Pr > 0.7$. The assumptions regarding the plate are:

(vi) homogeneous material of constant thermal properties,
(vii) one-dimensional conduction, and
(viii) no internal heat generation.

Model formulation

Boundary layers. Transient boundary layer equations for momentum and energy conservation in differential and integral forms, as well as an energy balance at the surface, were used in a previous study [1] to develop a system of three coupled ordinary differential equations for the hydrodynamic and thermal boundary layer thicknesses and surface temperature. Physically correct polynomial profiles of fourth order were assumed for flow velocity and temperature across the hydrodynamic and thermal boundary layers. The polynomials have time-dependent coefficients that adapt the profiles instantaneously, so they satisfy both the constant and time-dependent boundary conditions at each instant of time. In an attempt to include temperature-dependent fluid properties, the kinematic viscosity ν and thermal conductivity k were considered to vary linearly with the fluid temperature. This approach led to the equations presented below.

The hydrodynamic boundary layer thickness δ is governed by an ordinary differential equation with time t as the sole independent variable. The equation was expressed in terms of a dimensionless thickness Λ ($= C\delta^2/\nu_{f0}$) and a dimensionless time τ ($= Ct$).

$$\frac{d\Lambda}{d\tau}\frac{1}{20}\left[(\Omega_1+\Omega_2)\frac{1}{4}\Lambda-3\right] = -2+\Psi_1\Lambda-\Psi_2\Lambda^2-\Psi_3\Lambda^3 - \alpha_v(\theta_s-0.5)\left(2+\frac{(\Omega_1+\Omega_2)\Lambda}{6}\right) \quad (1)$$

where

$$\Omega_1=\frac{1}{U_{\infty *}}\frac{\partial U_{\infty *}}{\partial \tau}, \quad (2a)$$

$$\Omega_2=\frac{1}{C_*}\frac{\partial U_{\infty *}}{\partial x} \quad (2b)$$

and

$$\Psi_1=\frac{2}{15}\Omega_1+\frac{116}{315}\Omega_2, \quad (3a)$$

$$\Psi_2=\frac{1}{120}\Omega_1^2+\frac{71}{3780}\Omega_1\Omega_2+\frac{79}{7560}\Omega_2^2, \quad (3b)$$

$$\Psi_3=\frac{1}{4536}(\Omega_1+\Omega_2)^2\Omega_2 \quad (3c)$$

A transient ordinary differential equation was derived for the dimensionless surface temperature.

$$\frac{d\theta_s}{d\tau}=\frac{6}{Pr\,\Gamma}\left(\frac{q_{s*}\Gamma^{1/2}}{1+\alpha_k(\theta_s-0.5)}-2\theta_s\right) \quad (4)$$

where q_{s*} is a dimensionless heat flux defined below as

$$q_{s*}=\frac{q_s}{k\sqrt{C/\nu}\,(T_{s0}-T_\infty)} \quad (5)$$

The dimensionless thermal boundary layer thickness Γ $(=C\Delta^2/\nu_{f0})$ resulted from the following ordinary differential equation:

$$\frac{d\Gamma}{d\tau}\left(4-\frac{q_{s*}}{[1+\alpha_k(\theta_s-0.5)]\theta_s}\Gamma^{1/2}\right) = \frac{96}{Pr}-\Gamma^{1/2}\frac{28}{Pr}\frac{q_{s*}}{[1+\alpha_k(\theta_s-0.5)]\theta_s} - \Gamma^{3/2}f_1(\Lambda,\theta_s)+\Gamma^2 f_2(\Lambda,\theta_s)-\Gamma^{5/2}f_3(\Lambda,\theta_s) - \Gamma^3 f_4(\Lambda,\theta_s)+\Gamma^{7/2}f_5(\Lambda,\theta_s) + \frac{\alpha_k}{Pr}g(\Lambda,\theta_s) \quad (6)$$

where:

$$f_1=4\Omega_2\Lambda^{-1/2}+\frac{1}{3}\Psi_4\Lambda^{1/2} - \frac{1}{[1+\alpha_k(\theta_s-0.5)]\theta_s}\frac{dq_{s*}}{d\tau}, \quad (7)$$

$$f_2=\frac{1}{3}\left[\frac{8}{7}\Psi_4+\left(2\Omega_2\Lambda^{-1/2}+\frac{1}{6}\Psi_4\Lambda^{1/2}\right)\times\frac{q_{s*}}{[1+\alpha_k(\theta_s-0.5)]\theta_s}\right], \quad (8)$$

$$f_3=\frac{1}{7}\left[\frac{5}{4}\Psi_4\Lambda^{-1/2}-5\Omega_2\Lambda^{-3/2} + \frac{1}{2}\Psi_4\frac{q_{s*}}{[1+\alpha_k(\theta_s-0.5)]\theta_s}\right], \quad (9)$$

$$f_4=\frac{1}{7}\Lambda^{-1/2}\left[\left(\frac{4}{3}\Lambda^{-1/2}+\frac{q_{s*}}{[1+\alpha_k(\theta_s-0.5)]\theta_s}\right)\times\Omega_2\Lambda^{-1}-\left(\frac{2}{9}\Lambda^{-1/2} + \frac{1}{4}\frac{q_{s*}}{[1+\alpha_k(\theta_s-0.5t)]\theta_s}\right)\Psi_4\right], \quad (10)$$

$$f_5=\frac{5}{126}\frac{q_{s*}}{[1+\alpha_k(\theta_s-0.5)]\theta_s}\times\Lambda^{-1}\left(\Omega_2\Lambda^{-1}-\frac{1}{6}\Psi_4\right) \quad (11)$$

$$g=\frac{q_{s*}\Gamma^{1/2}}{[1+\alpha_k(\theta_s-0.5)]\theta_s}\times\left[20(\theta_s-0.5)+\frac{12\theta_s}{1+\alpha_k(\theta_s-0.5)} - \frac{6q_{s*}\Gamma^{1/2}}{[1+\alpha_k(\theta_s-0.5)]^2}\right] \quad (12)$$

and

$$\Psi_4=(\Omega_1+\Omega_2)\Omega_2 \quad (13)$$

The influence of the hydrodynamic boundary layer response on the transient thermal boundary layer thickness is included via advective terms appearing in the energy conservation equation. A time-dependent surface heat flux induces transients in the thermal boundary layer thickness as well, directly or via a time-dependent surface temperature.

The corresponding Nusselt number, when referenced to the jet width, was expressed as:

$$Nu_w=w\sqrt{\frac{C}{\nu}}\frac{q_{s*}}{\theta_s}\frac{1}{1+0.5\alpha_k[\theta_s(\tau)-1]} \quad (14)$$

Equation (14) indicates that Nusselt number is spatially constant, as expected in the stagnation region due to its symmetry.

Plate. The mathematical derivation of the temperature distribution across the plate is presented in detail, as it is the original part of the present analysis. The one-

dimensional transient heat diffusion equation for a constant thermal diffusivity a_p and no internal heat generation is:

$$\frac{\partial T_p}{\partial t} = a_p \frac{\partial^2 T_p}{\partial y^2} \tag{15}$$

where $T_p = T_p(y,t)$. The associated boundary conditions are

$$\textit{Bottom of the plate } (y=0): \quad -k_p \frac{\partial T_p}{\partial y} = q(t) \tag{16}$$

$$\textit{Impinging surface } (y=l_p): \quad T_p = T_s(t) \tag{17}$$

The heat diffusion partial differential equation (15) with time dependent boundary conditions (16) and (17) was decomposed in a steady-state equation and a pure transient equation. The former was associated with the constant part of the boundary conditions, and the latter with the variable part of the boundary conditions. The initial temperature distribution inside the plate, T_{p0} $(y, t=0)$ with $0 < y < l_p$, was assumed to be the steady-state $(\partial \cdot / \partial \tau = 0)$ solution of equation (15). The superimposed transient equation was solved by using a modified normal modes method described by Meirovitch [7]. This modified approach is based on the fact that a boundary-value problem consisting of a homogeneous differential equation with nonhomogeneous boundary conditions can be transformed into a problem consisting of a nonhomogeneous differential equation with homogeneous boundary conditions. According to this method, it was assumed that equation (15) has the following general solution in terms of θ_p $(= (T_p - T_\infty)/(T_{s0} - T_\infty))$, τ $(= Ct)$, and y_* $(= y/l_p)$:

$$\theta_p(y_*,\tau) = \theta_{p0} + \vartheta(y_*,\tau) + \pi(y_*)\big[q_*(\tau) - q_{*0}\big] + \xi(y_*)\big[\theta_s(\tau) - \theta_{s0}\big] \tag{18}$$

where

$$q_*(\tau) = \frac{q(\tau)}{(T_{s0} - T_\infty)\, k_p / l_p}, \tag{19}$$

$$\theta_{p0} = \theta_{s0} + (1 - y_*) q_{*0} \tag{20}$$

and $\theta_{s0} = 1$ by definition. Functions $\pi(y_*)$ and $\xi(y_*)$ were chosen to render the boundary conditions for $\vartheta(y_*,\tau)$ homogeneous. Thus,

$$\pi(y_*) = 1 - y_* \tag{21}$$

and

$$\xi(y_*) = y_*^2 \tag{22}$$

Equation (18) was introduced in equation (15), leading to a nonhomogeneous differential equation. Using modal analysis, the eigenvalue problem related to $\vartheta(y_*,\tau)$ yielded a solution as an infinite sum of orthogonal natural modes. The orthogonal property of modes was then invoked to reach an explicit form of the solution. The resulting time-dependent temperature distribution across the plate is given below.

$$\begin{aligned}\theta_p(y_*,\tau) &= -2\big[q_*(\tau) - q_{*0}\big] \sum_0^\infty \frac{\cos(\lambda_n y_*)}{\lambda_n^2} \\ &\quad - 2\big[\theta_s(\tau) - 1\big] \sum_0^\infty \frac{(-1)^n}{\lambda_n} \left(1 - \frac{2}{\lambda_n^2}\right) \cos(\lambda_n y_*) \\ &\quad + 2A \sum_0^\infty \left(\cos(\lambda_n y_*) \int_0^\tau \big\{ \big[q_*(s) - q_{*0}\big] \right. \\ &\qquad + (-1)^n \lambda_n \big[\theta_s(s) - 1\big] \big\} \\ &\qquad \left. \times \exp\big[-A\lambda_n^2(\tau - s)\big]\, \mathrm{d}s \right) \\ &\quad + (1 - y_*) q_*(\tau) + y_*^2 \theta_s(\tau) + 1 - y_*^2 \end{aligned} \tag{23}$$

where

$$\lambda_n = (2n+1)\frac{\pi}{2}, \quad n = 0, 1, 2, \ldots \tag{24}$$

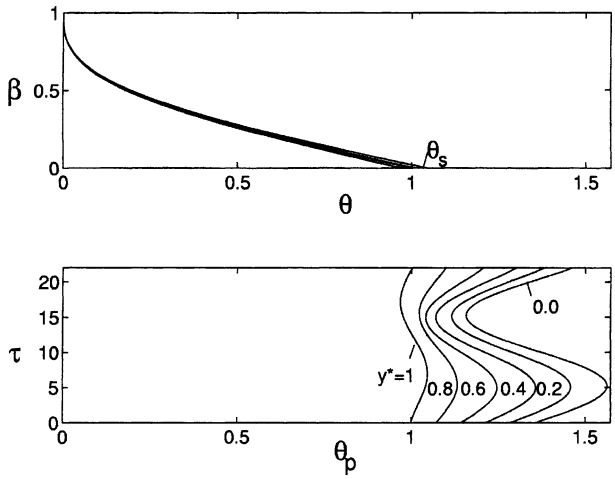

Figure 2. Selected instantaneous boundary-layer temperature profiles, adapted to time-dependent temperature distribution within the impinging plate, for $f_* = \varepsilon_1 = 0$, $f_{q*} = 0.05$, $\varepsilon_2 = 0.6$, $A = 0.004$, $B = 1.4$, $\alpha_v = \alpha_k = 0$, and $Pr = 0.7$.

Figure 2 illustrates temperature dynamics at selected locations across the plate, in conjuncture with temperature profiles within the thermal boundary layer. The profiles are shown to adapt in time to the instantaneous surface temperature, for a constant incident velocity and a

periodical heat flux applied at $y = 0$ (*figure 1*). Equation (23) allowed the computation of the heat flux $q_s(t)$ leaving the plate at the upper side ($y = l_p$, *figure 1*). According to Fourier's Law,

$$q_s = -k_p \frac{\partial T_p}{\partial y}\bigg|_{y=l_p} = -\frac{k_p}{l_p}(T_{s0} - T_\infty)\frac{\partial \theta_p}{\partial y_*}\bigg|_{y_*=1} \quad (25)$$

In dimensionless form (equation (5)), the surface heat flux encountered in equations (4) and (6)–(12) was given by:

$$q_{s*} = -B\frac{\partial \theta_p}{\partial y_*}\bigg|_{y_*=1} \quad (26)$$

where

$$B = \frac{k_p}{k_{f0}}\sqrt{\frac{\nu_{f0}}{C}}\,\frac{1}{l_p} \quad (27)$$

Forcing functions for freestream flow and applied heat flux

An important advantage of the present model is that boundary layer behavior can be predicted for any specified temporal variation in the incident velocity $V_i(t)$ (*figure 1*, via freestream velocity $U_\infty(t)$) or applied heat flux $q(t)$ (via $\theta_s(t)$ and $q_s(t)$), so long as the variations are piece-wise smooth. Transient terms were introduced by assuming that the dimensionless velocity gradient C_* ($= C_t w/V_i$) from potential flow theory remains unchanged and that unsteadiness in the incident velocity $V_i(t)$ induces temporal variations in the dimensional velocity gradient C_t ($= C_* V_i(t)/w$). The influences of the flow pulse characteristics and applied heat flux variations may be assessed by analyzing responses to different forcing functions for the dimensionless forms $U_{\infty *}(x_*, \tau)$ and $q_*(\tau)$. The only functional form considered in this study is a sinusoidal time-dependency, as specified by equations (28) and (29). The mathematical relations were chosen to insure the steady-state values at initial time ($\tau = 0$). For other functional forms, e.g., single ramps or periodic ramp-up/ramp-down pulses, the reader is sent to the paper of Mladin and Zumbrunnen [1].

$$U_{\infty *}(x_*, \tau) = C_* x_* \big[1 + \varepsilon_1 \cos(2\pi f_* \tau)\big] \quad (28)$$

$$q_*(\tau) = q_{0*}\big[1 + \varepsilon_2 \cos(2\pi f_{q*}\tau)\big] \quad (29)$$

It is important to note that $0 \le \varepsilon_{1,2} \le 1$, so as to avoid flow and heat reversals for which the model is not applicable.

Solution methodology and model verification

Runge–Kutta algorithms were implemented to obtain numerical solutions to the three ordinary, nonlinear differential equations (1), (4) and (6) for Λ, θ_s, and Γ. At each time-step, the temperature distribution inside the plate was computed with equation (23) and the resulting heat flux at the impingement surface (equation (26)) was introduced in the equations governing the flow. Representing the velocity and temperature profiles with temporally adaptive fourth-order polynomials restricted the numerical solutions to conditions for which the profiles remained physically realistic [8]. In general, the model eventually breaks down under a combination of high amplitude and high frequency fluctuations in the forcing functions.

Calculated steady-state Nusselt numbers were determined to be within 1% to 2.3% of those obtained by Evans [9] from the similarity solutions for a constant-property ($\alpha_k = 0$) flow past a wedge. Theoretical results were also validated against experiments performed with pulsating planar air-jets, as shown in *figure 3*. Model predictions for Nusselt number and dimensionless surface temperature were found close within about 1% to experimental measurements for periodic changes. A detailed comparison is provided in the next section.

3. RESULTS AND DISCUSSION

Model predictions for dimensionless heat flux leaving the surface (q_{s*}), dimensionless surface temperature (θ_s), and instantaneous Nusselt number scaled with its steady-state value ($Nu_* = Nu_w/Nu_0$) are compared in *figure 3* to experimental measurements. The experiments were performed with planar impinging air jet flows, using the experimental procedure and set-up described by Mladin [8]. The jet flow was issued at low turbulence from a convergent nozzle having an outlet opening of dimensions 5 mm × 50 mm; the flow impinged normally onto a plate made of aluminum nitride, a ceramic material of very high thermal conductivity (150 $\mathrm{W{\cdot}m^{-1}{\cdot}K^{-1}}$). This thermal property promoted a very nearly uniform temperature along the plate even for high amplitude transients in either flow velocity or applied heat flux. The plate had a surface of 100 mm × 50 mm and was 5 mm thick. The condition presented in *figure 3* pertained to a periodic change (e.g., pulse) in the incident velocity $V_i(t)$ and to a constant heat flux $q = q_0$ applied at the bottom of the

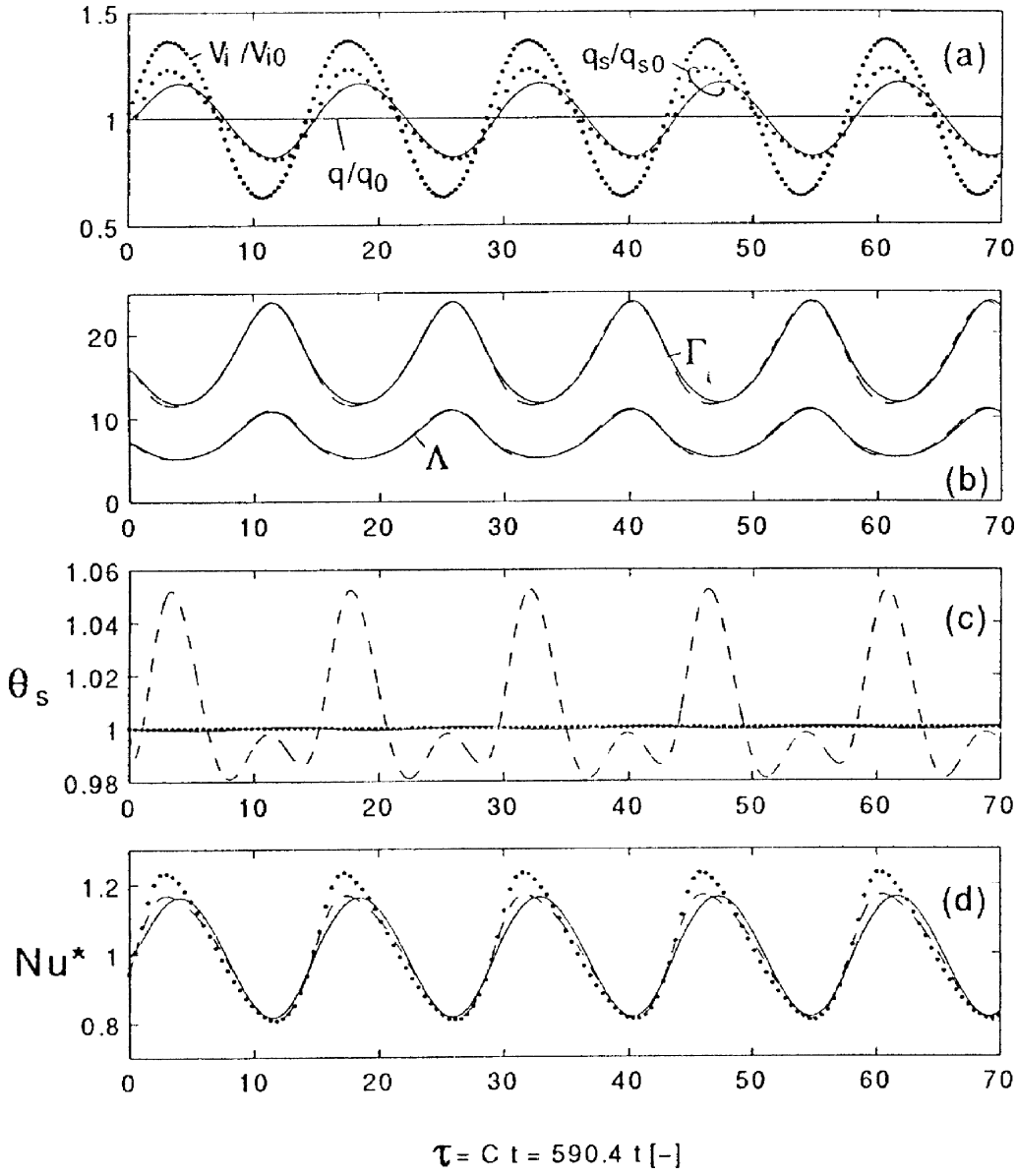

Figure 3. Comparison of model predictions to experimental measurements in an uniform planar air jet ($C_* = 0.785$, $Pr \cong 0.7$), for incident flow pulsations with $f_* = 0.07$ and $\varepsilon_1 = 0.36$, periodic heat flux variations with $f_{q*} = 0.07$ and $\varepsilon_2 = 0.22$, constant fluid properties ($\alpha_\nu = \alpha_k = 0$), and for $A = 0.004$, $B = 1.4$, and $Pr = 0.7$ ····· experimental, — — — model by Mladin and Zumbrunnen [1995], —— present model.

plate. Both $V_i(t)$ and $q_s(t)$ were measured in the stagnation plane (the system plane of symmetry) at a rate of 6 kHz and then converted to dimensionless forms. The dimensionless time step used for integration in the theoretical approach corresponded to the real time interval chosen for data sampling. The figure includes also the theoretical predictions computed with the model derived by Mladin and Zumbrunnen [1] for a zero-thick impinging plate (i.e., $q \equiv q_s$). In this case, errors of about 5% resulted in the theoretical dynamics of the dimensionless surface temperature. When the present model was used, measured and model-predicted values for q_{s*}, θ_s, Nu_* agreed on average to within 1%. However, larger departures (up to 10%) coupled with a small time lag are noted

around the points of maximum values; they may be attributed to some factors not encountered in the theoretical solution (see model assumptions) or due to the limited number of terms actually retained from the infinite summation in equation (23). Nevertheless, the general agreement of results gives credit to the predicted variations of boundary layer thicknesses, which, should be noted, are difficult to determine experimentally.

Since the novelty of the present model was the consideration of the heat diffusion through the plate, it was deemed appropriate to assess the influence of various parameters on the dynamics of the plate temperature distribution. This would further allow to reveal the plate influence on the boundary layer thicknesses and Nusselt number. For periodic forcing functions, it was noted that the plate temperature varied also periodically (*figure 2*). The panels of *figure 4* present the peak-to-mean temperature amplitude across the plate for specific parameter values. The temperature amplitude was computed relative to the mean temperature in order to make it more relevant. The value of unity represents, thus, a mean value. The results pertained to a sinusoidal freestream velocity and to a constant applied heat flux, as specified in the caption. Therefore, the fluctuations in the plate temperature propagated from the impingement surface ($y_* = 1$) to the bottom of the plate ($y_* = 0$). The temperature fluctuations at the bottom of the plate were found essentially zero ($< 1\%$), meaning that the penetration depth of the driving flow transients was less than the plate thickness. Notably, the temperature amplitude at the impinging surface was below 0.06, which affected the boundary layer thicknesses and Nusselt number to within 1% when compared to the theoretical results of Mladin and Zumbrunnen [1]. *Figure 4(a)* shows the influence of the nondimensional parameter A $(= a_p/(Cl_p^2))$, which incorporates the plate geometry and thermal diffusivity, as well as flow characteristics via freestream velocity gradient. The parameter A may also be regarded as the dimensionless penetration time for the heat conducted through the plate; it, thus, provides information about the natural (unforced) time response of the plate. Results indicated that the temperature fluctuations had higher amplitudes and penetrated deeper into the plate with increasing $A-$values, which was expected for higher plate thermal diffusivities (more responsive to heat conduction plate material).

Figure 4(b) presents the influence of another complex nondimensional parameter, B, which was defined in equation (27). For plates of lower B-values (e.g., lower thermal conductivities, thicker plates), the plate temperature was significantly more sensitive to the driving transients at the impingement surface due to a higher thermal inertia. Consequently, the temperature fluctuations had high amplitudes over longer distances from the impingement surface ($y_* = 1$) into the plate. By contrast, a low thermal inertia associated with high B-values determined a quick attenuation of already weak surface temperature fluctuations.

The influence of the fluid Prandtl number is illustrated in *figure 4(c)*. The steeper fluid temperature gradients at the surface, associated with the thinner boundary layers in higher Prandtl number fluids, acted as a stronger driving force for the plate temperature. It is predicted, thus, that flow pulses would rather induce significant temperature fluctuations at the impingement surface for water flows ($Pr \approx 6$) than for air flows ($Pr \approx 0.7$).

The flow pulse amplitude and frequency influenced the temperature fluctuations across the plate as it is shown in the last two panels of *figure 4*. Higher amplitudes of the driving flow pulses induced higher temperature fluctuations at the surface (*figure 4(d)*). By contrast, flow pulses of higher frequency induced lower fluctuations in the plate temperature (*figure 4(e)*). This result is associated with the thermal inertia of the plate and of the fluid as well. Mladin and Zumbrunnen [1] reported similar trends for the fluctuations in the hydrodynamic and thermal boundary layer thicknesses when the transients were induced by flow pulses of higher amplitude and of higher frequency, respectively.

Figure 5 illustrates a situation when both the incident velocity and applied heat flux had a sinusoidal temporal variation (equations (28) and (29)). The forcing functions were chosen of different frequencies ($f_* < f_{q*}$), but of same amplitude ($\varepsilon_1 = \varepsilon_2$), in order to compare the induced fluctuations in the system dependent variables. Compared to *figure 4*, the plate temperature displayed strong fluctuations at the bottom of the plate (*figure 5(a)*), as a result of the time-dependent boundary condition at $y_* = 0$ (equation (16)). Despite of the periodic flow, which insured another time-dependent boundary condition at $y_* = 1$ (equation (17)), the temperature fluctuations decreased in magnitude and had the extreme points shifted with increasing y_*. The shift is attributed to the difference in forcing frequencies. In fact, the heat flux leaving the plate is shown in *figure 5(b)* to display only the forcing frequency pertaining to the flow (f_*), although it was computed from the plate temperature gradient at the impingement surface equation (26). The surface temperature $\theta_s = \theta_p$ ($y_* = 1$) fluctuations alone were too weak to induce fluctuations of frequency f_{q*} in the boundary layer and Nusselt number dynamics (*figures 5(c) and 5(d)*). Otherwise said, the flow and heat transfer coefficient did not appar-

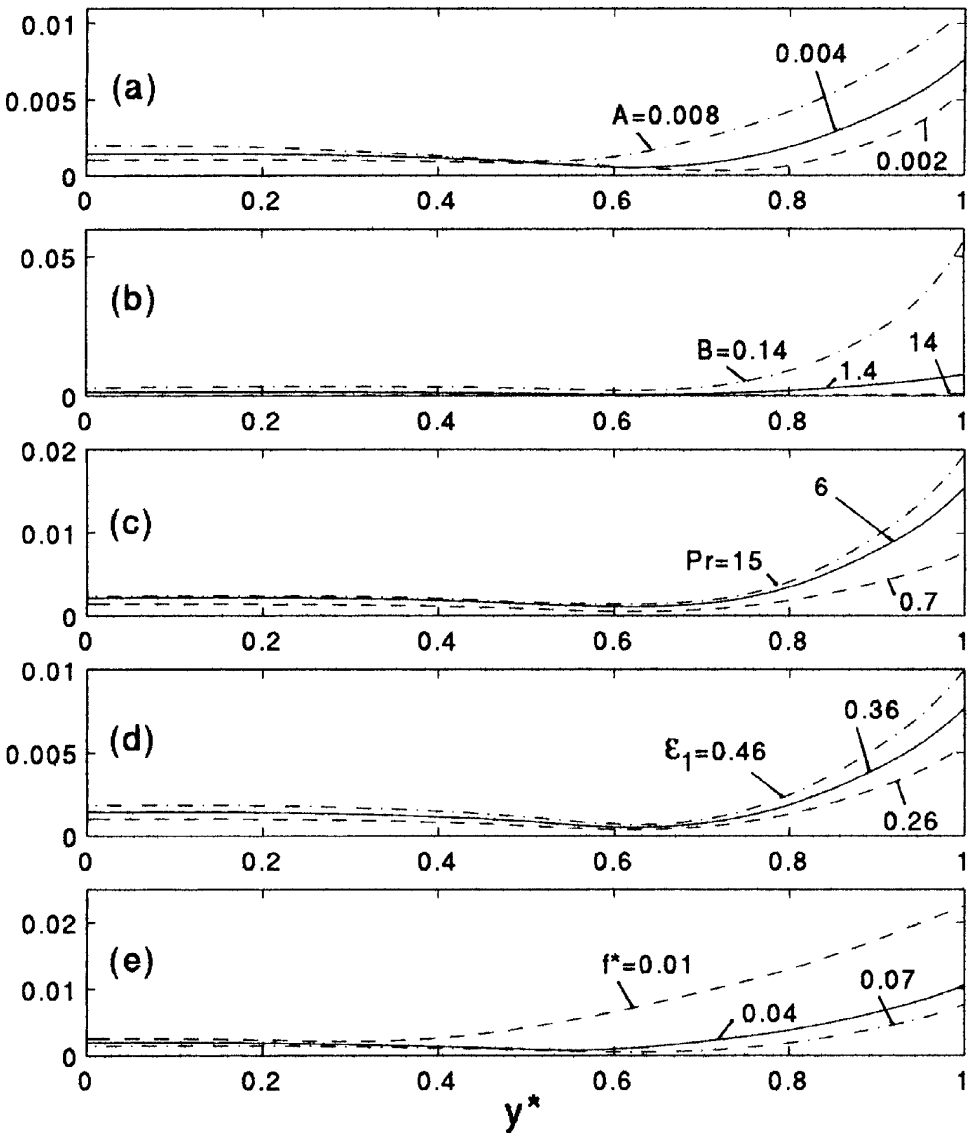

Figure 4. Influence of various parameters on the temperature fluctuation amplitude across the plate for sinusoidal flow pulsations, constant applied heat flux ($\varepsilon_2 = 0$), and constant fluid properties ($\alpha_v = \alpha_k = 0$). If not otherwise specified, the parameters are: $f_* = 0.07$, $\varepsilon_1 = 0.36$, $A = 0.004$, $B = 1.4$, and $Pr = 0.7$.

ently sense the transients in the applied heat flux, except for the fluid temperature at the impingement surface.

Results pertaining to a constant incident velocity but periodic temporal variations in the applied heat flux indicated that the boundary layer thicknesses and Nusselt number were not essentially affected. For example, Λ, Γ, and Nu_* deviated from the initial steady-state values with less than 1% for a heat flux amplitude as high as 60%. However, the plate temperature distribution was affected in a manner similar to that presented in *figure 2*, displaying a decreasing amplitude with increasing distance from the bottom of the plate.

4. CONCLUSIONS

A mathematical model was derived to reveal the influence of the plate temperature dynamics on the hydrodynamic and thermal boundary layer thicknesses and

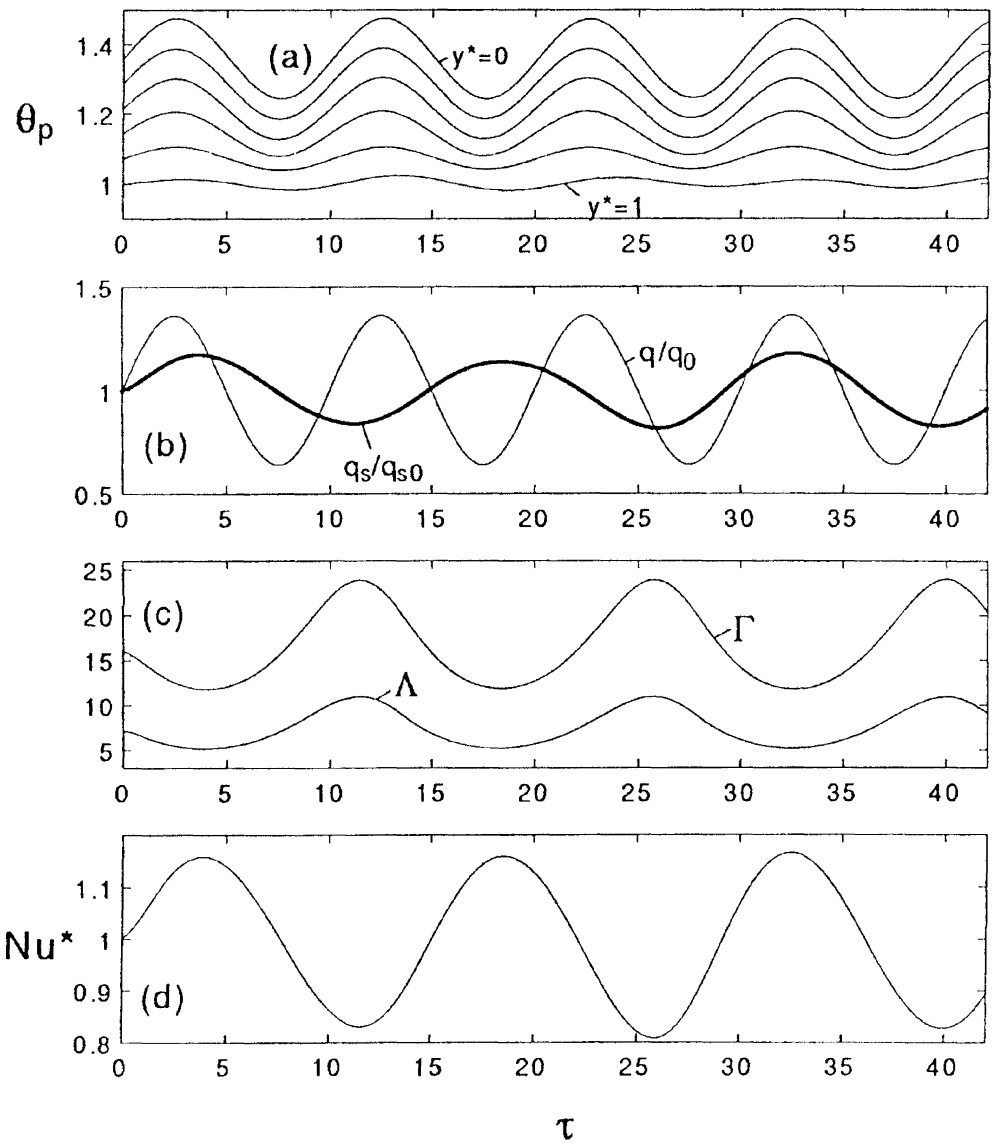

Figure 5. Response due to sinusoidal flow pulsations and sinusoidal heat flux variations for constant properties ($\alpha_v = \alpha_k = 0$) and $f_* = 0.07$, $\varepsilon_1 = 0.36$, $f_{q*} = 0.1$, $\varepsilon_2 = 0.36$, $A = 0.004$, $B = 1.4$, and $Pr = 0.7$.

Nusselt numbers for a planar stagnation flow, when incident velocity and/or applied heat flux are transient. Under unsteady flow conditions but constant applied heat flux, the model predicted an unsteady heat flux transferred to the fluid. The characteristics of this induced unsteadiness were altered by plate properties and geometry. The model was validated by an agreement between theoretical predictions and experimental data to within 1%. The study showed that the boundary layer thicknesses and Nusselt number were affected to within 1% by heat flux periodical variations of amplitude ε_2 as high as 0.6. By contrast, the temperature across the impinging plate had significant fluctuations induced by both forcing functions. Therefore, the present model is deemed particularly useful to predict the dynamics of the plate for different parameter values.

Interesting results may result when one of the two dimensionless forcing frequencies (f_*, f_{q*}), or both, correspond to the natural time response ($A = a_p/(C \cdot l_p^2)$) of the impinging plate to heat conduction, to the fluid viscous diffusion time δ^2/ν or to the fluid thermal dif-

fusion time $\Delta^2(\rho c_p/k)_f$. Consideration of fluid property variation with temperature (via α_v and α_k) was also included in the presented model. With temperature-dependent kinematic viscosity, the response of the hydrodynamic boundary layer had a time lag of about $\tau = 2$ for $-0.2 < \alpha_v < 0.05$, which includes temperature dependencies representative of air and water. A temperature dependence for the fluid thermal conductivity had little effect on the thermal boundary layer and Nusselt number responses within the range $0.05 < \alpha_k < 2.5$, with dynamics nearly identical compared to the constant property case.

The model may be used also to study the nonlinear effects in the instantaneous and time-averaged values for boundary layer thicknesses and Nusselt number. The small corrected fluctuations in surface temperature may render the dynamics of these variables chaotic, as suggested in a previous work [10].

REFERENCES

[1] Mladin E.C., Zumbrunnen D.A., Dependence of heat transfer to a pulsating stagnation flow on pulse characteristics, J. Thermophysics Heat Tran. 9 (1) (1995) 181–192.

[2] Kasza K.E., Thermal response characteristics of unsteady stagnation point flows: a new approach, Internat. J. Heat Mass Tran. 18 (1975) 329–331.

[3] Sheriff H., Zumbrunnen D.A., Effect of flow pulsations on the cooling effectiveness of an impinging planar water jet, J. Heat Trans. 116 (1994) 886–895.

[4] Mladin E.C., Zumbrunnen D.A., Local convective heat transfer to submerged pulsating planar jets, Internat. J. Heat Mass Tran. 40 (14) (1997) 3305–3321.

[5] Hansen A.G., Similarity Analysis of Boundary Value Problems, Prentice-Hall, Englewoog, Cliffs, NJ, 1964.

[6] Zumbrunnen D.A., Transient convective heat transfer in planar stagnation flows with time-varying surface heat flux and temperature, J. Heat Tran. 114 1 (1992) 85–93.

[7] Meirovitch L., Analytical Methods in Vibrations, MacMillan, New York, 1994, pp. 301-308.

[8] Mladin E.C., Instantaneous convective heat transfer to pulsating submerged jets, Ph.D. thesis, Clemson University, Clemson, South Carolina, 1995.

[9] Evans H.L., Mass transfer through laminar boundary layers 7. further similar solutions to the B-equation for the case $B = 0$, Internat. J. Heat Mass Tran. 5 (1962) 35–37.

[10] Mladin E.C., Zumbrunnen D.A., Nonlinear dynamics of hydrodynamic and thermal boundary layers in laminar stagnation flows, J. Thermophysics Heat Trans. 8 (3) (1994) 514–523.